Bull. Mater. Sci., Vol. 39, No. 4, August 2016, pp. 1133–1138. © Indian Academy of Sciences.
DOI 10.1007/s12034-016-1226-7

Electric properties of textured $(K_{0.44}Na_{0.52}Li_{0.04})(Nb_{0.86}Ta_{0.10}Sb_{0.04})O_3$ thick film prepared by screen printing method

FANG FU[1], JIWEI ZHAI[2,*] and ZHENGKUI XU[3]

[1]Luoyang Institute of Science and Technology, Luoyang 471023, China
[2]Functional Materials Research Laboratory, Tongji University, Shanghai 200092, China
[3]Department of Physics and Materials Science, City University of Hong Kong, Kowloon Tong, Hong Kong

MS received 20 September 2015; accepted 8 February 2016

Abstract. **Textured $(K_{0.44}Na_{0.52}Li_{0.04})$ $(Nb_{0.86}Ta_{0.10}Sb_{0.04})O_3$ thick film was fabricated by the screen printing method with plate-like $NaNbO_3$ particles as template. Thick film with 75% grain orientation was prepared. Remnant polarization and coercive field observed from the *P–E* loops of textured thick film were 3.6 μC cm^{-2} and 21 kV cm^{-1}, respectively. Textured $(K_{0.44}Na_{0.52}Li_{0.04})$ $(Nb_{0.86}Ta_{0.10}Sb_{0.04})O_3$ thick film exhibited diffusion behaviour by analysing the temperature dependence of permittivity and loss tangent. The result of leakage current density showed a conduction mechanism of Schottky emission. Piezoelectric (PZT) properties of the thick film were characterized by the relationship of unipolar strain and applied electric field and the PZT constant d^*_{33} of textured thick film reached to 150 pm V^{-1}. Nonlinear PZT property of the thick film was investigated by Rayleigh law.**

Keywords. **Screen printing; ferroelectricity; piezoelectricity; nonlinear property.**

1. Introduction

The interest in piezoelectric (PZT) thick films is driven by various applications including microactuators, microelectromechanical systems (MEMS), high-frequency transducers, pyroelectric infrared sensors and surface acoustic wave devices [1–3]. PZT film can offer an attractive option for MEMS technology owing to its superior PZT properties; however, the toxic nature of Pb restricts its development. As a result, a substitute, an environmental-friendly material, for PZT becomes an urgent demand. $K_{0.5}Na_{0.5}NbO_3$-based (KNN) perovskite materials are considered to be one of the most promising candidates for its high Curie temperature (T_c = 420°C) and better PZT property (d_{33} is approximately 80 pC N^{-1} with conventional sintering) [4]. However, its PZT properties is still worse than PZT materials. Some measurements such as composition modification and grain orientation technique were applied to improve the PZT properties of KNN-based materials [5–8]. The research of lead-free ceramics focus on KNN-based ceramics specially after Saito *et al*'s [9] research on textured $(K_{0.44}Na_{0.52}Li_{0.04})(Nb_{0.86}Ta_{0.10}Sb_{0.04})O_3$ (KNN) ceramics. Textured KNN ceramics exhibits an excellent PZT property which seem to compete with PZT.

Screen printing is a traditional process that is suitable for fabricating films with thickness of larger than 15 μm and suitable for MEMS technique. It is a good method to produce integrated electronics devices [10–13].

Screen printing method was used to prepare textured KNN thick film with plate-like $NaNbO_3$ particles as template to obtain a thick film with high PZT properties. The structure and electric properties of the thick film were investigated and the nonlinear PZT property was analysed by Rayleigh law.

2. Experimental

KNN thick film was designed with a textured structure for improving its PZT property. However, KNN prepared by traditional method does not exhibit preferential property. Thus, an anisotropy template is necessary. $Na_{2.5}Bi_{2.5}Nb_4O_{15}$ possess plate-like shape which is suitable for a template material. If Bi in $Na_{2.5}Bi_{2.5}Nb_4O_{15}$ is eliminated by displacement reaction, a plate-like $NaNbO_3$ was obtained and would act as a template for KNN thick film. The detailed experimental process is described below.

First, plate-like $Bi_{2.5}Na_{2.5}Nb_4O_{15}$ particles with a thickness less than 1 μm and a width about 10 μm (as shown in figure 1a) were synthesized by heating Bi_2O_3, $NaCO_3$ and Nb_2O_5 in NaCl molten salt according to equation (1). Plate-like $NaNbO_3$ particles were then prepared by the molten salt method with plate-like $Bi_{2.5}Na_{2.5}Nb_4O_{15}$ particles and $NaCO_3$ as raw materials according to equation (2)

$$5Bi_2O_3+5Na_2CO_3+8Nb_2O_5 = 4Na_{2.5}Bi_{2.5}Nb_4O_{15}+5CO_2\uparrow, \quad (1)$$

$$Na_{2.5}Bi_{2.5}Nb_4O_{15} + Na_2CO_3 + 0.25Nb_2O_5 = 4.5NaNbO_3 + 1.25Bi_2O_3 + CO_2\uparrow. \quad (2)$$

*Author for correspondence (apzhai@tongji.edu.cn)

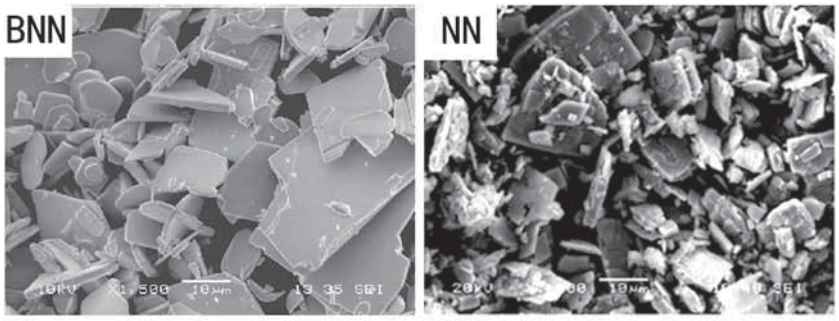

Figure 1. SEM image of plate-like (**a**) $Bi_{2.5}Na_{2.5}Nb_4O_{15}$ particles and (**b**) $NaNbO_3$ particles.

$NaNbO_3$ particles have a thickness of about 1 μm and a width ranging from 5 to 10 μm as shown in figure 1b. Second, reagent-grade K_2CO_3, Na_2CO_3, Nb_2O_5, $LiSbO_3$ and Ta_2O_5 powders were mixed and ball-milled with ethanol as a medium for 24 h. The mixture was dried and annealed at 800°C for 2 h to form matrix powder. A mixture of 80 wt% matrix powder and 20 wt% plate-like template was milled for 3 h in an agate mortar with ethanol as medium for agitating and then the organic vehicle was added in the mixture to mill for another 2 h in the same mortar to form screen printing paste. A glass rod was placed in the paste and lifted up. If the paste forms a continues line, then the viscosity of paste is well-ajusted. The organic vehicle was composed with terpineol and ethyl cellulose in the ratio of 10 : 1. The prepared paste was printed by using a screen with 200 meshes on the Al_2O_3 substrate with Ag–Pd bottom electrode to form a green thick film. The green thick film is composed of five layers as one green layer is too thin (about 6 μm) to get a compact thick film. Green film was dried at 90°C and pressed by isostatic pressing at 200 MPa. Finally, the film was annealed at 600°C for 5 h to remove the organic substance and then sintered at 1150°C for 2 h at the rate of 3°C min^{-1}.

Phase structure of the film was examined by using X-ray diffraction (XRD, Bruker D8 Advanced, Germany) with CuKα radiation. Surface and cross-section morphologies of the film were observed by using scanning electron microscopy (SEM, JSM EMP-800). Degree of the grain orientation was characterized by using Lotgering's factor, which was calculated by the following formula [14]:

$$F = (P - P_0)/(1 - P_0), \tag{3}$$

where P is the sum I (h 0 0)/sum I (h k l), P_0 the sum I_0 (h 0 0)/sum I_0 (h k l). Sum I is the summation of XRD peak intensities of the sintered specimen. Sum I_0 is the summation of XRD peak intensities of the equiaxed reference powders (see JCPDS card 19-1221).

To measure the electric properties of the thick film, gold electrodes with a thickness of 80 nm and diameters of 0.5 mm and 2 mm (2 mm for measurement of longitudinal displacement field curves) were sputtered. Temperature dependences of permittivity and loss tangent were measured by using a high-precision LCR meter (HP 4284A). Leakage current density of the films was measured with Keithley 6517A Electrometer (Cleveland, OH). P–E hysteresis loops and longitudinal displacement field curves were evaluated by a ferroelectric test system (Precision Premier II, USA) connected with a Miniature Plane-mirror Interferometer and accessory Laser Interferometric Vibrometer (Germany).

3. Results and discussion

3.1 *Phase structure and microstructure*

Figure 2a–c shows the XRD pattern and SEM images of the film sintered at 1150°C. The intensities of (h00) peaks were increased relatively strong than those of other peaks when compared with the XRD patterns of the equiaxed powders (JCPDS no. 19-1221). This result indicates a grain orientation along (h00) after treatment at 1150°C. On the basis of XRD pattern, the degree of grain orientation was calculated, and Lotgering's factor is about 75%. This (h00) grain orientation is supposed to form by the guidance of NN template. Normally, three key factors are known to determine the template grain growth (TGG) process in bulk ceramic: template content, template size and sintering temperature. The grain growth of textured ceramics is generally controlled by three factors, including particle densification, growth along the printing direction of templates at the expense of matrix grains, and template thickening after ceasing growth along printing direction [15,16]. A similar growth behaviour was also observed in KNN thick film. It is well known that defects on boundary are high-energy points and easy to deposit other particles to reduce its surface energy. Therefore, the matrix grains were absorbed on the defects of template and grow longitudinally with the defects position. Because of the different sizes of matrix and templates, the matrix with small size and high-energy grain boundary was absorbed by the large template grains and finally formed a brick-like morphology as shown in figure 2b and c. The thick film is composed of two types of grains: irregularly shaped grains (marked as 'a'), which are matrix grains, and plate-like grains arranged parallel to the screen printing direction (marked as

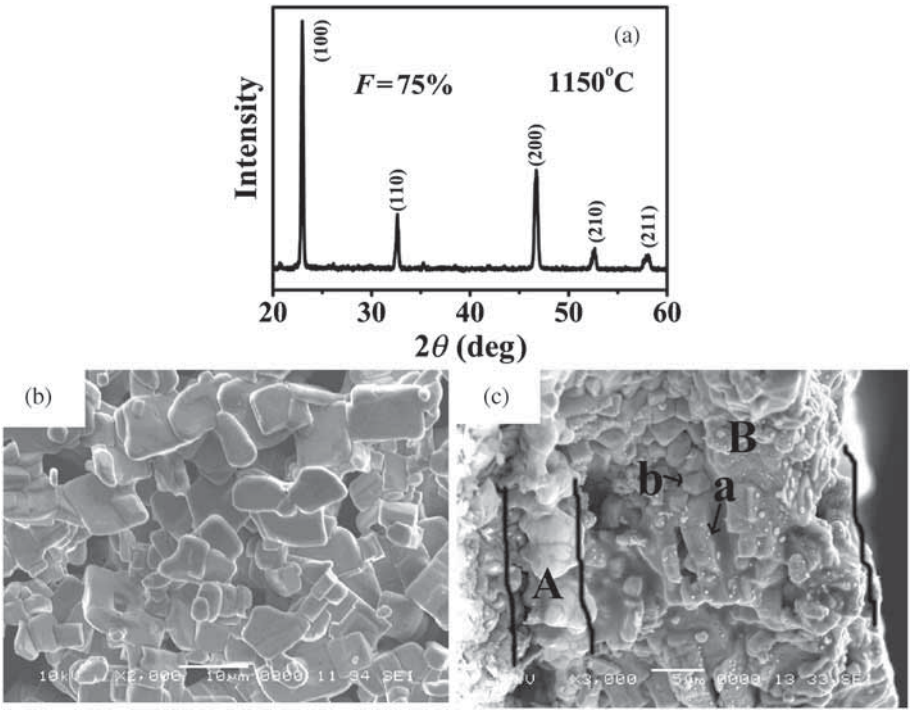

Figure 2. (**a**) XRD pattern, (**b**) surface microstructure photographs and (**c**) cross-section of the KNN textured thick film.

'b'). Plate-like grains with the size of ∼5 μm were observed. Pores distributed in thick film are not only resulted by the large amount of inorganic substance in green film but also by the volatilization of K and Na in the 1150°C sintering The thick film was grown on a Ag–Pd electrode (marked as 'A') as shown in figure 2c and has a thickness of about ∼20 μm (marked as 'B').

3.2 *Electrical properties*

Electrical properties of the thick film were investigated and are depicted in figure 3. Figure 3a shows the plots of polarization *vs.* electric field of the textured film. Its behaviour is different from that of bulk ceramic which exhibits typical saturated polarization behaviour. The hysteresis loops of the film were represented by an unsaturation curve with a remanent polarization of 3.6 μC cm^{-2} and a coercive field of 21 kV cm^{-1}. These values are much lower than those of the bulk ceramic. It is possibly resulted by the existence of high porosity which observed from SEM image This porosity microstructure caused a high leakage current indicated by arc sharp of P–E loop. Further, this film will breakdown with the application of higher electric field.

Figure 3b shows the temperature dependence of the permittivity at different frequencies (1–1000 kHz). The temperature dependences of permittivity depict a typical phase diffusion behaviour with a broaden peak. A modified empirical expression, Curie–Weiss law, which was proposed by Uchino *et al* [17] has been applied to quantify the diffuseness of a phase transition:

$$\frac{1}{\varepsilon_r} - \frac{1}{\varepsilon_c} = \frac{(T - T_c)^\alpha}{C}, \tag{4}$$

where ε_r and ε_c are the permittivity at temperature T and the maximum permittivity at Curie temperature T_c, respectively. The parameter α is called a diffusion exponent ranging from 1 to 2 for the materials with a diffuse phase transition. The value of α can be obtained from the slope of the linear relationship between $\ln(1/\varepsilon_r - 1/\varepsilon_c)$ and $\ln(T - T_c)$ as shown in the inset of figure 3b. The diffusion exponent α was 1.56 at 100 kHz. The phase diffusion of the thick film may ascribe to the compositional fluctuation or structural disorder due to the introduction of $LiSbO_3$ and Ta_2O_5. Substitution with $LiSbO_3$ and Ta_2O_5 can originate lattice distortion of perovskite structure [18,19]. In addition, the volatilization of K and Na also contributed to the compositional fluctuation. The permittivity of the film is lower than that of the bulk ceramics, which possibly caused by the poor microstructure of the film. The pores distributed in the thick film as shown in figure 2b can be considered as a second phase, thus, the permittivity was diluted by this low-permittivity phase and consequently resulted in the lower permittivity compared with the bulk ceramics.

Figure 3c shows the relationship between leakage current density and applied electric field of the thick film. Leakage current density of KNN thick film at 50 kV cm^{-1} less than 5×10^{-6} A cm^{-2}. The literature identifies three possible leakage current limiting mechanisms: Schottky emission,

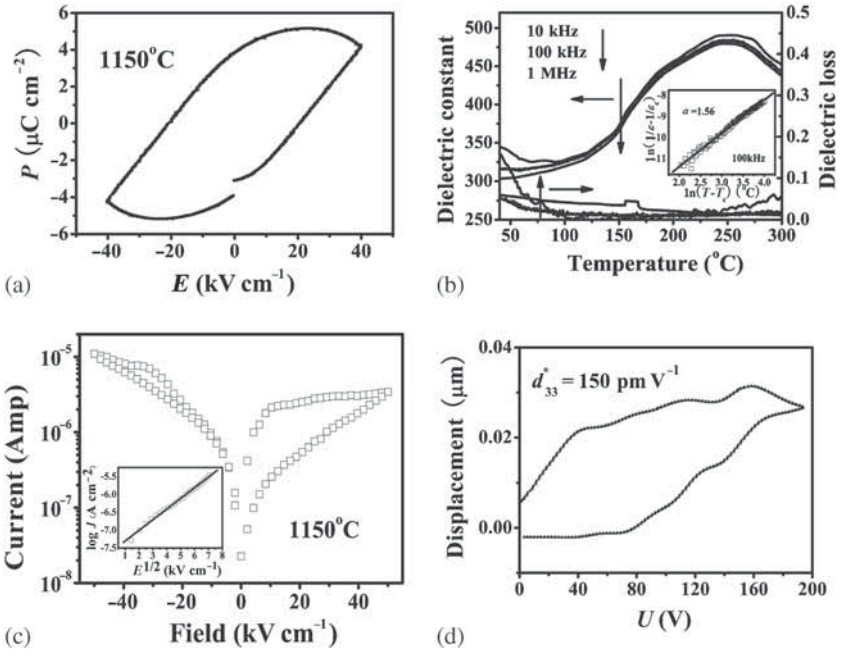

Figure 3. (**a**) P–E hysteresis loops of the thick films, (**b**) temperature dependences of permittivity and loss of the thick film, (**c**) relationship between leakage current density and applied electric field and (**d**) relationship of the unipolar strain and the applied electric field.

Poole–Frenkel effect and space charge limited current (SCLC). Schottky emission is interface-limited, while both Poole–Frenkel effect and SCLC are bulk-limited. The Schottky emission current density for insulators, in which the electronic mean-free path is less than the insulator thickness, is given by

$$J = AT^2 \exp\left[\frac{-q(\varphi_b - \sqrt{qE/4\pi\varepsilon_0\varepsilon_i})}{kT}\right], \tag{5}$$

where J is the leakage current density, A the Richardson constant, T the absolute temperature, ε and ε_i the permittivity of free space and the optical permittivity of the film, respectively, k Boltzmann's constant, Φ_b the height of the Schottky barrier and E the electric field at the interface. A linear relationship was observed by plotting $\ln(J)$ *vs.* $E^{1/2}$ for Schottky emission mechanism. Similarly, SCLC mechanism and Poole–Frenkel emission can also be characterized by a linear relationship of J *vs.* E^2 and $\ln(J)$ *vs.* $E^{1/2}$ [20–23]. The curve of current density J *vs.* E^2 does not follow a straight line, which indicates that the thick film is not ruled out by SCLC mechanism here. The straight lines are obtained by plotting $\ln(J)$ *vs.* $E^{1/2}$, which agrees well with equation (2). However, the linear relationship of $\ln(J)$ *vs.* $E^{1/2}$ presented both for Schottky emission and Poole–Frenkel effect. The Poole–Frenkel mechanism was resulted from defects and irrelevant with the type of electrode and Schottky emission was controlled by the surface of electrode and thick film. Because of the different heights of Schottky barrier for top golden electrode and bottom Ag–Pd electrode, the J *vs.* E curve should present in an asymmetric fashion for Schottky emission. The J *vs.* E curve of the thick film showed an asymmetric sharp as shown in figure 3c, which indicated the Schottky emission conduction mechanism for the textured thick film.

Figure 3d shows the curves of displacement *vs.* voltage for the textured thick film at room temperature. Nonlinear strain as a function of electric field is observed. The PZT strain constant can be calculated by the formula $d_{33} = S_{max}/E_{max}$ in which S_{max} and E_{max} represent as the maximum value of strain (displacement) and electric field (voltage), respectively. The calculated value was 150 pm V^{-1} for the textured film which can compare with PZT thick film ($\sim$180 pm V^{-1}) [24]. This high PZT characteristic may be related to the preferred grain orientation in the film. However, this value is substantially lower than that of the bulk ceramic. One possible reason is the clamping effect of the substrate. Another possibility is large quantity of defects which reflected by large hysteresis in figure 3d. The domain boundary motion might be partially pinned, which contribute to high levels of hysteresis as shown in figure 3d.

3.3 *Nonlinear dielectric properties*

Effects of the domain-wall pinning on dielectric properties are of substantial interest in recent years. A detailed theoretical study of the domain-wall pinning named Rayleigh law was developed to describe the nonlinear induced magnetic response of ferromagnetic materials due an applied magnetic field [25,26]. Hall [27] expanded the use of Rayleigh model in ferroelectrics to consider the nonlinearity of the dielectric

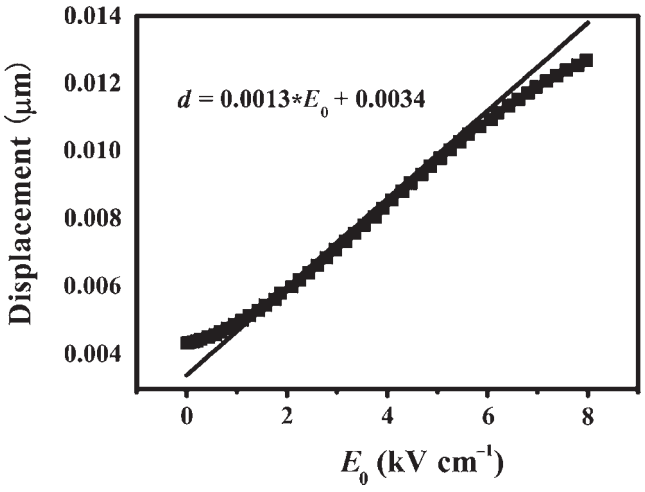

Figure 4. Displacement for the thick film measured as a function of applied field.

response under an applied electric field and evaluated the real and imaginary contributions to the dielectric and PZT responses.

In the Rayleigh region, the displacement will increase linearly with the amplitude of the applied electric field, E_0.

$$d(E_0) = d_{\text{init}} + \alpha E_0, \tag{6}$$

where the Rayleigh parameter is d_{init}, which is the initial reversible PZT response at zero electric field, including the intrinsic and reversible internal interface motion; the PZT Rayleigh coefficient α is the irreversible motion of internal interfaces. At a fixed field, αE represents the irreversible extrinsic contribution and the ratio of $\alpha E_0/(d_{\text{init}} + \alpha E_0)$ quantifies the ratio of irreversible response to total PZT response [28,29].

The field dependence PZT responses of textured KNN thick film were quantified using the method mentioned above as shown in figure 4. The thick film obeys Rayleigh law within suitable field regions (generally, $0 < E < E_c/2$). Rayleigh parameters for PZT responses were calculated from fits to the linear portions of the data. The thick film exhibited linear Rayleigh behaviour over the range of $1< E <$ 6 kV cm^{-1} The ratio of $\alpha E/(d_{\text{init}} + \alpha E)$ was found to be 28–75% with E = 1–6 kV cm^{-1} This value indicated that irreversible response, which induced a large hysteresis in S–E curve as shown in figure 3d, dominates PZT response in textured thick film with E increase The irreversible component mainly ascribed to the interaction between pinning centres and domain walls. The value of $\alpha E_0/(d_{\text{init}} + \alpha E_0)$ presents the irreversible extrinsic contributions to the thick film PZT response, which consequently resulted from clamping effect of substrate and high defect concentration of the thick films. As a volatile element, KNN-based materials may leave the samples to form vacancies in the lattice during sintering at high temperature. The volatilization of K and Na in textured KNN thick films can cause a deviation of chemical stoichiometry and defect/domain interaction, which consequently influences the defect states. The dipolar defects can be assumed to be K and Na vacancies–oxygen vacancies defects. These dipolar defects lead to a clamping of the domain walls by anisotropic centres.

4. Conclusions

(*h*00)-textured KNN thick film was successfully fabricated on Ag–Pd buffer Al_2O_3 substrates by the screen printing method. Lotgering's factor of the thick film reached 75%. Remanent polarization and coercive field of the textured thick film were 3.6 μC cm^{-2} and 21 kV cm^{-1}, respectively. A diffusion behaviour was observed in the thick films and the diffusion exponent was calculated as 1.56. Conduction mechanism displays the transition of Schottky emission. PZT constant d_{33}^* of the thick film was 150 pm V^{-1}, which can be compared with PZT thick film. Finally, the ratio of $\alpha E_0/(d_{\text{init}} + \alpha E_0)$ was found to be 28–75% with E_0 = 1–6 kV cm^{-1}, which indicated that the dominated PZT response in textured thick film was irreversible extrinsic contribution on large electric field.

Acknowledgements

We would like to acknowledge the support from the National Natural Science Foundation of China under grant nos. 50972108 and 50932007. The work was also partially supported by the Research Grants Council of the Hong Kong Special Administrative Region, China (City University No. 103307).

References

[1] Rao C V M and Prasad G 2012 *Bull. Mater. Sci.* **4** 579
[2] Bah M, Giovannelli F and Schoenstein F 2015 *Ultrasonics* **63** 23
[3] Shin D J, Jeong S J and Seo C E 2015 *Ceram. Int.* **41** S686
[4] Egerton L and Dillon D M 1959 *J. Am. Ceram. Soc.* **42** 438
[5] Wiegand S, Flege S and Baake O 2012 *Bull. Mater. Sci.* **5** 745
[6] Haugen A B, Olsen G H and Madaro F 2014 *J. Am. Ceram. Soc.* **97** 3818
[7] Koruza J, Rozic B and Cordoyiannis G 2015 *Appl. Phys. Lett.* **106** 202905
[8] Pavlic J, Malic B and Rojac T 2014 *J. Am. Ceram. Soc.* **5** 1497
[9] Saito Y, Takao H and Tani T 2004 *Nature* **423** 84
[10] Wang M Y, Ma W B and Chen N 2015 *Mater. Lett.* **152** 17
[11] Lei A, Xu R C and Borregaard L M 2014 *J. Microelectromech. System* **4** 842
[12] Wei Y, Torah R and Yang K 2013 *Sens. Actuators A—Phys.* **203** 241
[13] Fu F, Shen B and Zhai J W 2011 *J. Alloys Compd.* **509** 7130
[14] Lotgering F 1959 *J. Inorg. Nucl. Chem.* **9** 113
[15] Gao F, Hong R and Liu J 2010 *J. Electroceram.* **24** 145

[16] Shoji T, Fuse K and Kimura T 2009 *J. Am. Ceram. Soc.* **92** S140
[17] Uchino K and Nomura S 1982 *Ferroelectr. Lett. Sec.* **44** 55
[18] Qian S H, Zhun K J and Pang X M 2014 *Ceram. Int.* **40** 4389
[19] Tang H, Zhang M F and Zhang S J 2013 *J. Eur. Ceram. Soc.* **33** 2491
[20] Hiruma Y, Aoyagi R and Nagata H 2005 *Jpn. J. Appl. Phys.* **44** 5040
[21] Zhang S T, Kounga A B and Aulbach E 2007 *Appl. Phys. Lett.* **91** 112906
[22] Yang H, Jain M and Suvorova N A 2007 *Appl. Phys. Lett.* **91** 072911
[23] Shang D S, Wang Q and Chen L D 2006 *Phys. Rev. B* **73** 245427
[24] Osone S, Brinkman K and Shimojo Y 2008 *Thin Solid Films* **12** 4325
[25] Damjanovic D and Demartin M 1996 *J. Phys. D: Appl. Phys.* **29** 2057
[26] Neel L 1942 *Cah. Phys.* **12** 1
[27] Hall D A 2001 *J. Mater. Sci.* **36** 4575
[28] Vendrell X, García J E and Rubio-Marcosc F 2013 *J. Eur. Ceram. Soc.* **33** 825
[29] Bhattacharyya S, Saha S and Krupanidhi S B 2002 *Thin Solid Films* **422** 155